Available online at www.sciencedirect.com
ScienceDirect
Journal of Nuclear Materials 358 (2006) 164–175
journal of nuclear materials
www.elsevier.com/locate/jnucmat

Tungsten bronze-based nuclear waste form ceramics. Part 3: The system $Cs_{0.3}M_xW_{1-x}O_3$ for the immobilization of radio cesium

Vittorio Luca *, Elizabeth Drabarek, Harriet Chronis, Terry McLeod

Australian Nuclear Science and Technology Organisation, Institute of Materials and Engineering Sciences, PMB 1, Menai, NSW 2234, Australia

Received 17 January 2006; accepted 26 June 2006

Abstract

Previous studies in this series have indicated that Cs- and Sr-loaded Mo-doped hexagonal tungsten bronze (MoW-HTB) oxides, either in the form of fine grained powders, or as composite granules, can be converted to leach resistant ceramics at modest temperatures in the range 600–1200 °C. In the present study it has been shown that such waste form ceramics can also be readily prepared through very simple conventional routes involving the blending of cesium nitrate with tungstic acid and other oxide components followed by heating in air. The phase chemistry resulting from the blending of these oxides has been explored. In the $Cs_{0.3}M_xW_{1-x}O_3$ compositional system where x = Ti, Zr, Nb and Ta the solid solution limit has been found to be where $x = 0.2$. For all values of x between 0 and 0.2 mixed phase materials of HTB and WO_3 were obtained and Cs was found associated with HTB phases that are both rich and depleted in M element. At temperatures above about 1000 °C, phase pure HTB compounds in the space group *P*63/*mcm* were obtained. Even when x greatly exceeds 0.2, the additional oxide content did not interfere with the formation of the HTB phase. Durability of the $Cs_{0.3}M_xW_{1-x}O_3$ compositions as gauged by the fractional Cs loss in de-mineralized water was lowest when M = Ti and Nb, and greatest when M = Zr. From these results the durability appears intimately linked with the unit cell a-dimension which in turn varies with M cation radius.

1. Introduction

It was demonstrated in parts 1 and 2 of this series that microcrystalline hydrated hexagonal tungsten bronze (HTB) materials in the form of finely divided powders or as composite HTB-polyacrylonitrile granules can be used for the simultaneous and selective extraction of Cs^+ and Sr^{2+} from acidic fission product containing simulant solutions [1,2]. Additionally, it has also subsequently demonstrated that these materials could then be converted to highly leach resistant ceramics by heating in air to moderate temperatures in the range 600–1200 °C [3]. At still higher temperatures melting produces highly durable materials with little or no Cs volatilization and a tolerance to the presence of Mo. While this

* Corresponding author.
E-mail address: vlu@ansto.gov.au (V. Luca).

0022-3115/$ - see front matter
doi:10.1016/j.jnucmat.2006.06.019

'cradle-to-grave' option for dealing with radiogenic Cs and Sr is a potentially powerful manner of dealing with radiotoxic isotopes, it is not necessarily the only or favoured option. If other partitioning strategies such as solvent extraction are used to yield a fission product stream devoid of U, Pu and minor actinides and having Cs-137 and Sr-90 as the main radioactive isotopes, such a stream would still require recourse to some form of immobilization that is effective for a period of at least ten halve lives. An alternative to passing this fission product solution through a column of inorganic ion exchanger is to directly blend the solution with waste form oxide precursors, remove excess water and sinter or hot press to form a ceramic multiphase assemblage. An alternative to sintering or hot pressing is of course to melt to give a glass. The radiotoxic elements become immobilized in ceramic host phases by substitution or form part of the glass matrix. In either the case of glass or ceramic the radiotoxic elements are rendered relatively insoluble.

Perhaps the most well known ceramic technology is synroc, whose development was pioneered mainly by Australian government agencies. Synroc is a titanate-based ceramic containing mineral phases such as hollandite, for sequestration of Cs; zirconolite, for sequestration of a variety of actinides, lanthanides and strontium; and perovskite for Sr. Although the production of synroc is more complex than that of glass waste forms, it is generally accepted that the leach resistance of the synroc ceramic matrix is superior to that of glass [4–6].

Prior to the development of glass waste forms by US agencies, considerable effort was aimed at developing tailored ceramic waste forms. Hatch [7] and then later McCarthy et al. appear to have been among the first to propose the incorporation of HLW calcines in ceramic materials including zirconium titanates- and apatite-based materials [8–10]. In McCarthy's 'supercalcines' Sr, Si, Ca, and Al oxides were mixed with HLW calcines and heated in air to about 1200 °C to form a finely crystalline phase assemblage that had comparable leach resistance to HLW-containing borosilicate glass. During the period 1970–1985 Dosch et al. developed titanate sorbents which could take up radioactive elements from various solutions and which could then be converted on heating to stable ceramic waste forms [11].

Some other non-glass waste forms which have been developed, but have been less considered, are geopolymer materials [12,13] and materials produced by gelation [14]. Glass Crystal Composites (GCC) which combine some of the advantages of both glass and crystalline materials have also been quite extensively studied by US agencies since the 1960s [15–19].

Of all the radioactive elements produced by nuclear fission, arguably one of the most problematic is cesium. Two isotopes are relevant Cs-137 and Cs-135. Cesium-137 decays to metastable Ba-137 with $t_{1/2} = 30.17$ years which then decays to stable Ba with $t_{1/2} = 2.552$ min and the emission of an energetic gamma ray photon. Cesium-135 which on the other hand is extremely long lived ($t_{1/2} = 2.3 \times 10^6$ years) is a beta emitter. While cesium-137 has a relatively short half-life compared with some of rare earth elements that are produced, it is responsible for most of the radioactivity in fission product materials once other more short-lived radioisotopes have decayed away. These nuclear properties, together with high aqueous solubility, make cesium at the least troublesome, and at most, deadly. For example, trace quantities of Cs-137 from the Chernobyl nuclear disaster are to be found in southern hemisphere crops. Such dispersion is unlikely to occur for the other elements such as the actinides which tend to form dense insoluble compounds. Slightly less problematic because of its lower solubility is the beta emitter Sr-90 which has a comparable half-life to Cs-137 and contributes in a significant way to the radioactivity in the 0–300-year period.

The mineral phase in which cesium is immobilized in synroc is titanate hollandite and there are relatively few other materials that can boast the performance of this mineral phase. Indeed studies abound that attest to the leach resistance of Cs-hollandites in de-ionized water. Strontium is immobilized in the perovskite titanate and its performance is inferior to that of hollandite.

The objectives of the present investigation are to explore the possibility that tungsten bronze-based waste forms can be produced using simple methods, detail the phase chemistry, assess the compositional flexibility of this potential waste form system and evaluate the performance of the resultant materials. The method employed involves the simple mixing of aqueous Cs-nitrate solutions with tungstic acid H_2WO_4 to form a slurry which is calcined at relatively low temperatures air to form compositions of the type $Cs_yM_xW_{1-x}O_3 \cdot ZH_2O$. Such compositions allow the testing of the compositional flexibility of the basic bronze framework as a host for

radiocesium. They also allow an assessment of the variations in performance that accrue on M for W substitution.

2. Description of structures and their synthesis

The main structures that are relevant to this work are summarized in Fig. 1. The hydrothermally prepared, microcrystalline adsorbents that were the subject of earlier ion exchange investigations have structures corresponding to the hexagonal tungsten bronzes HTB (Fig. 1(c)) and pyrochlores PYR (Fig. 1(d)) [1]. They are part of a larger family of group V and VI transition metal oxides that comprise oxides whose frameworks are made up of corner-sharing octahedra containing tungsten, niobium, tantalum, molybdenum and so forth. In addition to the two hexagonal members, HTB and PYR, which contain 3- and 6-membered ring tunnels, there also exists the cubic bronze CB (Fig. 1(a)) which contains only 4-membered ring tunnels and a tetragonal tungsten bronze (TTB) with 3-, 4-, and 5-membered ring tunnels (Fig. 1(b)). These latter phases are not known to be ion-exchangers in the sense that, to the authors' knowledge, it has never been demonstrated that the tunnel cations can be replaced by other cations from the solution phase. Titanate analogues of both CB and PYR are well known in the synroc context with CB being the direct tungstate analogue of the cubic perovskites. Likewise the HTB material can be considered as an analogue of hollandite in the sense that both frameworks contain tunnels that are sufficiently large to accommodate Cs. It is probably worth noting however that the 6-membered ring tunnels of HTB are smaller, and accommodate Cs more snugly, than the 8-membered ring tunnels of edge and corner sharing octahedra in hollandite. Furthermore, the plane of corner-sharing octahedra defining hexagonal tunnels in the *c*-axis direction of HTB is similar to the Zr-containing structural subunit which can be found in the highly durable ceramic zirconolite. One may therefore wonder if such a structural subunit is not at least partially responsible for the stability of the aforementioned ceramic materials. This possibility could be addressed through computations of lattice energies using sophisticated computer codes.

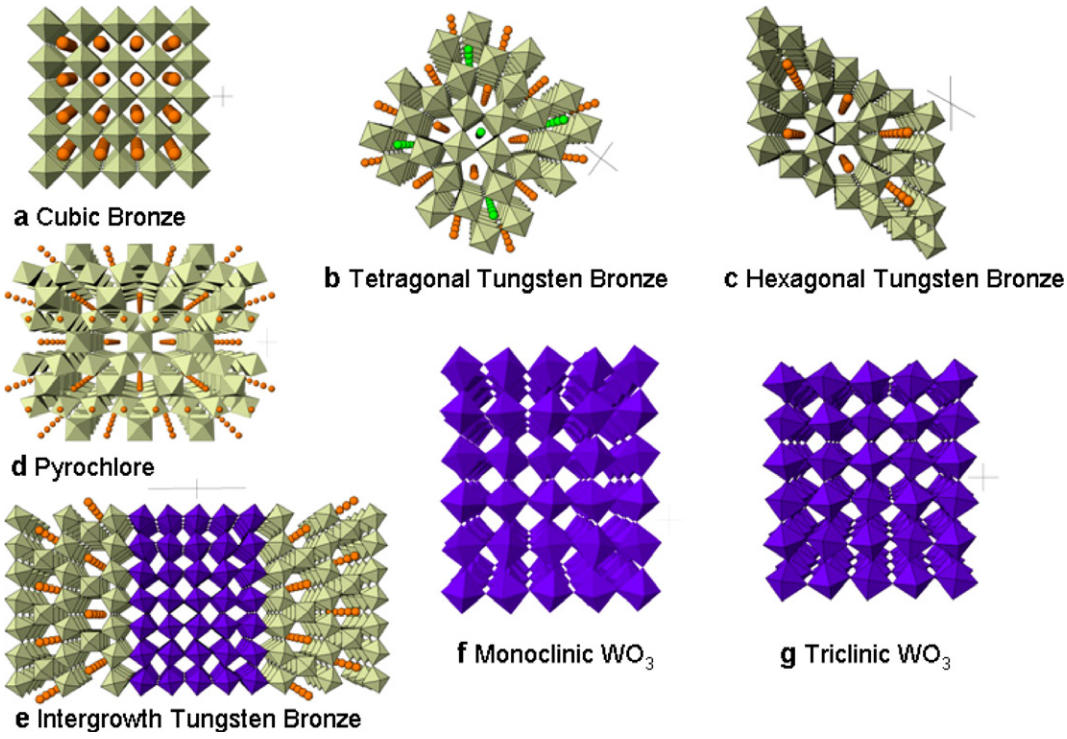

Fig. 1. Structures of relevant tungsten oxides: (a) cubic (perovskite) bronze (CB), (b) tetragonal tungsten bronze (TTB), (c) hexagonal tungsten bronze (HTB), (d) cubic pyrochlore (PYR), (e) intergrowth tungsten bronze (ITB), (f) monoclinic WO_3, (g) triclinic WO_3. Phases f and g are only the WO_3 phases that are stable at near room temperature.

In addition to the structures described above, which relate mostly to the phases in which radionuclides can be located before and after heating, a number of other tungstate phases need to be considered which may additionally form during heating of the radionuclide loaded sorbents. The structures of many of these oxides are based on distorted ReO_3 frameworks as is the cubic bronze described above. The structures of Fig. 1(e)–(f) consist mostly of corner sharing octahedral frameworks with empty square tunnels, or in other words, they may be referred to as 'empty frameworks'. They differ in the degree of distortion arising mainly from octahedral tilting. Interesting structural transformations occur between these empty framework structures as a function of temperature. For instance below −17 °C the monoclinic P*c* phase is stable, from 17 to 330 °C the monoclinic WO_3 $P2_1/n$ is stable, from 330 to 740 °C the orthorhombic WO_3 *Pmnb* is stable and from 740 to 900 °C the tetragonal WO_3 *P*4/*nmm* is stabilized.

The intergrowth tungsten bronze (ITB) (Fig. 1(g)) is a special composite structure in that it contains structural elements from HTB and the empty framework phases which are repeated at regular intervals.

Gerand et al. [20] were the first to synthesize hydrous tungsten trioxide compounds with a hexagonal tungsten bronze-like structure through wet chemical methods. The compound they synthesized also possessed hexagonal tunnels and a very similar structure to hexagonal tungsten bronze compounds but with orthorhombic symmetry and containing structural water molecules as indicated by the formula $WO_3 \cdot 1/3H_2O$. Related compounds were later described by Figlarz et al. [21] who also discussed thermally driven structural transformations in empty-tunnel orthorhombic $Mo_xW_{1-x}O_3$ compounds. The hexagonal-type orthorhombic $WO_3 \cdot 1/3H_2O$ shows fairly high thermal stability to about 300 °C after which it converts to a supermetastable hexagonal WO_3 compound, and then, at about 500 °C, to thermodynamically stable monoclinic WO_3 [22]. These transformations are classed as reconstructive as there is a change in the secondary coordination of the WO_6 polyhedra without any change in primary coordination, i.e., bonds must be broken. It is presumably water in the hexagonal tunnels that stabilizes the initial hydrated orthorhombic structure.

The ternary system A_2O–WO_2–WO_3 with A = Li, Na, K, Rb and Cs has been previously explored by Cava et al. [23]. In their study of the A_2O–WO_2–WO_3 phase diagram they reported two new oxides with the composition $Cs_{8.5}W_{15}O_{48}$ (HTB-type) and CsW_2O_6 (pyrochlore).

Castro et al. [24] has reported the synthesis of polycrystalline powders of $ATi_{0.5}Te_{1.5}O_6$ (A = K, Rb, Cs, Tl), $ATi_{0.5}W_{1.5}O_6$ (A = Rb, Cs, Tl), and $CsM_{0.5}W_{1.5}O_6$ (M = Zr, Hf) with defect cubic pyrochlore structures (*Fd*-3*m*), $Z = 8$. They also observed a linear relationship between the unit cell *a*-parameters and the ionic radii of the A cations, as well as the average ionic radii of the M atoms. Thus, at least in the pyrochlore structure, the substitution of Ti, Zr and Hf for W is established.

3. Experimental

For the high temperature phases with general composition $Cs_yM_xW_{1-x}O_3$, cesium nitrate (Aldrich) was used as received and dissolved in a minimum amount of de-mineralized water and then combined with tungstic acid (H_2WO_4, Aldrich). Tungstic acid is a free flowing finely divided yellow powder and when combined with the $CsNO_3$ solution a free-flowing slurry resulted. To this slurry was added additional precursor powder materials such as TiO_2, ZrO_2 and Nb_2O_5 and Ta_2O_5. The TiO_2 was prepared by addition of titanium isopropoxide (Aldrich) to water to form a precipitate which was filtered, washed and dried at 70 °C. The resulting powder was finely ground and its water content established in order to properly calculate stoichiometries. The $Cs_yM_xW_{1-x}O_3$ compositions were heated in air at temperatures in the range 600–1300 °C. For temperatures below about 1200 °C where partially sintered masses were produced these were ground and sieved to 10–35 μm for leach testing using a modified PCT procedure. To produce consolidated crystalline masses from which disks-shaped samples were cut for MCC-1 leach testing, compositions were calcined at 1300 °C for (M = Zr, Ti, Mo, Ta) and 1400 °C (M = Nb).

MCC-1 leach tests were carried out in de-ionized water and a number of different pH solutions at 90 °C for 7–84 days, using disks that were 10 mm in diameter and 2 mm high. At least duplicates were used in all leach tests with quadruplets used in most tests up to 84 days. All samples required for leach testing were prepared by machining using non-polar and chemically inert fluids, so preleaching was minimized, and the large surfaces of the samples were polished to a 0.25 μm diamond powder finish.

Leachate solutions were analyzed using inductively coupled plasma–mass spectrometry (ICP–MS). The leach periods were 0–7, 7–28, 28–56, 56–84 days. The leachates were cooled to ambient room temperature, filtered (0.45 μm), and the pH measured at the end of each leach period. The leachates were then acidified with concentrated nitric acid (3 wt%) so the final pH of the leachant was approximately 0.5. The leachates were replaced for each sample at the beginning of each leach period. The normalized release rate was calculated by dividing the cumulative extraction by the time leached and the element matrix normalization. As the variability in release rate between samples (under the same conditions) was larger than the uncertainties in measuring each element, the values reported were the average values and error bars on the graphs represent one standard deviation from the average.

Normalized Cs release rates ($g/m^2/day$) were determined according to the relationship in Part 1. The surface area was commonly calculated from the geometric area of a polished pellet if a strict MCC-1 protocol was followed but may be the surface area measured by the BET method if a powdered material was used (PCT). For MCC-1 tests a geometric surface area to solution volume SA/$V = 0.1\ cm^{-1}$ was used. For PCT tests using powders we used a V/m ratio of 100 ml/g.

Unless otherwise stated elemental releases from powder materials were determined by loading 0.2 g of powdered sample into a 45 ml Teflon-line autoclave to which was added 20 ml of de-mineralized water to give a volume-to-mass ratio, $V/m = 100$ (ml/g). The sealed autoclaves were heated in a fan-forced oven in which the temperature was controlled to ±1 °C. The cooled supernatant solutions were filtered through a 0.2 μm filter and analysed by inductively coupled plasma–mass spectrometry (ICP–MS). For experiments in which elemental releases were measured as a function of pH, nitric acid and sodium hydroxide were used to achieve the required pH. The fraction of Cs released, f, was determined as in Part 1.

Survey X-ray powder diffraction patterns were recorded on a Scintag X1 diffractometer using Cu K_α radiation and a Peltier detector. Data for unit cell refinements were recorded on a Panalytical X'Pert Pro diffractometer using the same wavelength radiation and employing a solid state detector utilizing real time multiple strip technology. Thermogravimetric analyses (TGA) and differential thermal analsyses (DTA) were conducted simultaneously on a Setaram TAG24 (France) instrument. Secondary and backscattered electron images were obtained on a Jeol JSM6400 scanning electron microscope (SEM) operating at 15 keV. Energy dispersive spectroscopy (EDS) analyses of the various phases observed were obtained with a Noran Voyager (Noran) EDS system. Surface area measurements were performed on a Micrometrics ASAP 2010 instrument.

4. Results

4.1. Phase chemistry

Since a thorough examination of all synthetic parameters in the $Cs_yM_xW_{1-x}O_3$ system would be prohibitively time consuming we chose to fix y at 0.3 (for Cs^+), which approaches the maximum theoretical limit for a monovalent cation in the hexagonal tungsten bronze system. Only limited values x of were investigated and only four substitutional elements, M, were examined (Ti, Zr, Ta and Nb) in this study with the emphasis being on Ti. The suite of M elements chosen was based on the likelihood of achieving M for W substitution and their applicability in a nuclear waste management context. Loading with higher amounts of Cs, while possible, was not considered practically relevant since in a real waste form material high loadings of $^{137}Cs^+$ could cause excessive heat load.

Another issue that is relevant to the preparation of usable waste form materials is volatilization of Cs. This volatility was gauged by examination of the data presented in Table 1 where XRF analyses of targeted nominal $Cs_yM_xW_{1-x}O_3$ compositions were compared to those found by XRF analyses as a function of calcination temperature. It was apparent that even for compositions that were melted at 1300 and 1400 °C there is negligible loss

Table 1
XRF analyses of selected compositions as a function of calcination temperature

T (°C)	Target	Found
90	$Cs_{0.3}Nb_{0.40}W_{0.60}O_3$	$Cs_{0.18}Nb_{0.37}W_{0.63}$
750	$Cs_{0.3}Nb_{0.40}W_{0.60}O_3$	$Cs_{0.19}Nb_{0.35}W_{0.66}$
1000	$Cs_{0.3}Nb_{0.40}W_{0.60}O_3$	$Cs_{0.19}Nb_{0.39}W_{0.60}$
1300	$Cs_{0.3}Nb_{0.20}W_{0.80}O_3$	$Cs_{0.25}Nb_{0.36}W_{0.64}$
90	$Cs_{0.3}Zr_{0.30}W_{0.70}O_3$	$Cs_{0.39}Zr_{0.42}W_{0.58}$
750	$Cs_{0.3}Zr_{0.30}W_{0.70}O_3$	$Cs_{0.31}Zr_{0.36}W_{0.64}$
1000	$Cs_{0.3}Zr_{0.30}W_{0.70}O_3$	$Cs_{0.30}Zr_{0.33}W_{0.67}$
1400	$Cs_{0.3}Zr_{0.20}W_{0.80}O_3$	$Cs_{0.30}Zr_{0.26}W_{0.74}$

of Cs. This augurs extremely well for actual application.

There is a paucity of literature on the formation of HTB materials with composition $Cs_yM_xW_{1-x}O_3$ and so their preparation in air was not assured. Therefore, we undertook the preparation of $Cs_{0.3}Ti_{0.6}W_{0.4}O_3$ at temperatures in the range 600–1400 °C to first ascertain the effect of temperature on the resultant phase assemblage. The XRD patterns of the phases are shown in Fig. 2. The samples heated to between 600 and 800 °C were poorly crystalline but showed some evidence of the presence of HTB phases (marked by diamonds in pattern of Fig. 2(c)). In addition, the major reflections of anatase and rutile were identified along with those indicative of a cubic pyrochlore phase. For temperatures at or above 900 °C, patterns of HTB phases became more pronounced and defined, and the overall complexity diminished as temperature was increased. The patterns of the samples calcined between 900 and 1100 °C were relatively phase pure as judged from the XRD patterns showing only evidence of HTB and rutile. For the patterns of the samples heated to 1200 °C (Fig. 2(g)) and above, an additional cubic pyrochlore pattern was observed with the major reflections of this phase indicated by the arrows at about 13° and 20° 2θ. Unreacted rutile was also tentatively identified in the pattern of the sample heated to 1300 °C. For the single phase pattern of Fig. 2(f) it was possible to achieve an excellent Rietveld refinement of the pattern (Fig. 3) and thus get accurate lattice parameters of the associated HTB phase ($P6_3/mcm$; $a = 7.332$, $c = 7.813$).

The back scattered electron image of a cross-section of the composition heated to 600 °C in air

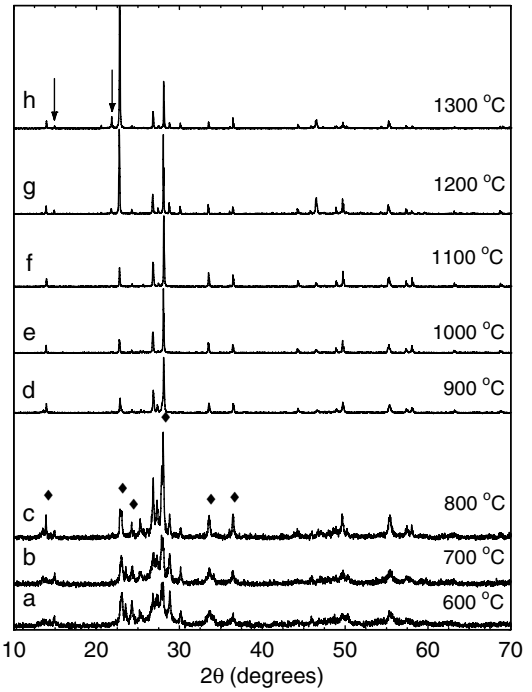

Fig. 2. XRD patterns of $Cs_{0.3}Ti_{0.6}W_{0.4}O_3$ compositions heated to increasing temperatures: (◆) HTB phase, (arrows) PYR phase.

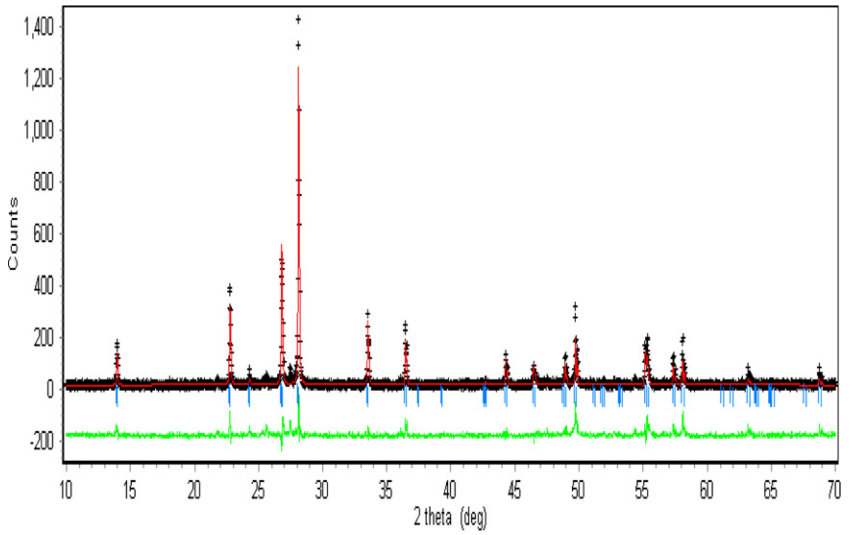

Fig. 3. Reitveld refinement of nominal composition $Cs_{0.3}Ti_{0.6}W_{0.4}O_3$ heated in air at 1100 °C. Unit cell parameters are $a = b = 7.3316$, $c = 7.8128$ in hexagonal space group $P63/mcm$.

is shown in Fig. 4(a). Three compositions were revealed by spot EDS analysis. Phase 1, in dark contrast, was TiO_2 which is also clearly identified in the XRD patterns of Fig. 2(c). Phase 2 was a Cs-rich tungstate having a fibrous morphology characteristic of HTB and a very low level of Ti substitution. The fibrous morphology is particularly evident in high magnification images. Phase 3 had no distinct morphology, a high Cs loading and high levels of substitutional Ti.

As the heating temperature was gradually increased the amount of Ti substituted into the Cs-containing HTB phase was also found to increase up to a limit of about 16 at.% of the total framework elements. SEM micrographs of cross-sections of the samples heated at 1200 °C in air are shown in Fig. 4(b). Two phases were clearly identified from these micrographs. The first was a phase with stoichiometry that was consistent with a Cs-containing uniformly Ti-substituted HTB (regions 1–3) while the second corresponded to unreacted titania. Extensive EDS analysis of this sample revealed that the majority of particles present exhibited compositions containing Cs, Ti and W of similar composition. Thus, the SEM analysis supported the phase homogeneity indicated by XRD. This was also the case for the sample heated to 1300 °C which is above the melting temperature of the phase assemblage. Furthermore, it was apparent that the unreacted titania precursor possessed considerable porosity.

With the temperature fixed at 1000 °C, which was the point at which well defined patterns were evidenced for the $Cs_{0.3}Ti_{0.6}W_{0.4}O_3$ compositions, the Ti content was varied for the starting compositions (Fig. 5). The XRD pattern of the sample with $x = 0$ (Fig. 5(a)) was quite complex and the distinct reflections of an HTB phase were tentatively identified in

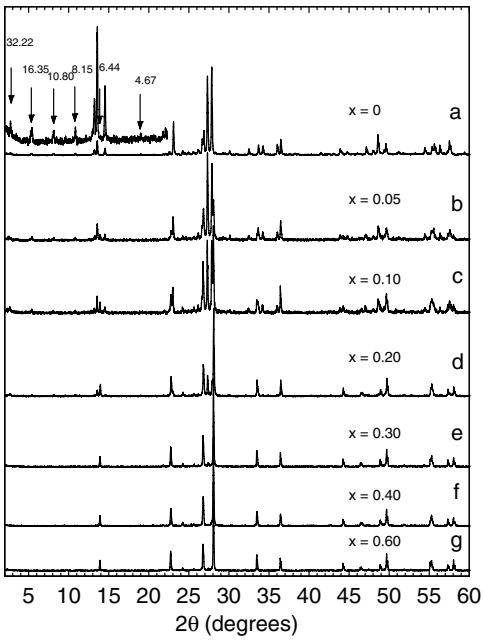

Fig. 5. XRD patterns of $Cs_{0.3}Ti_xW_{1-x}O_3$ compositions heated at 1000 °C with x values ranging from 0 to 0.6.

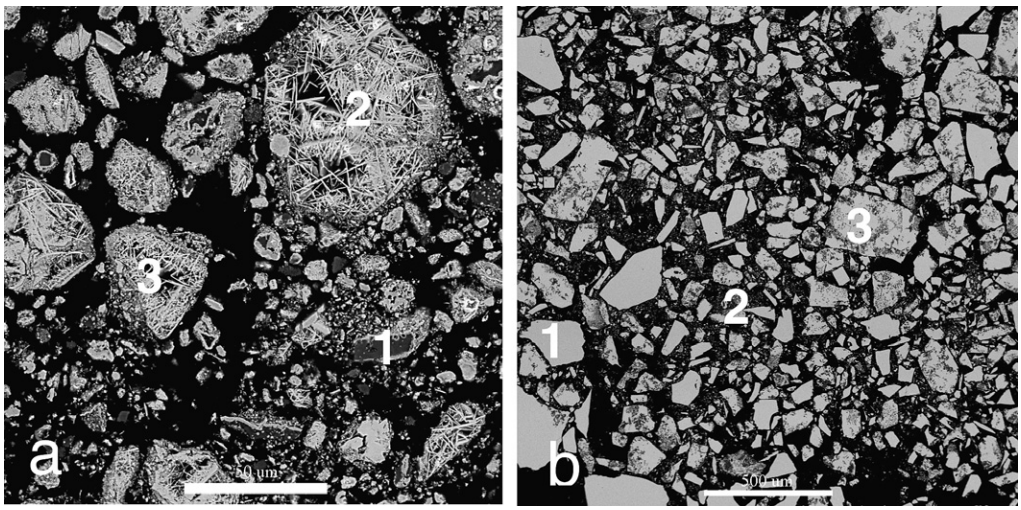

Fig. 4. Cross-sectional back scattered electron images of $Cs_{0.3}Ti_{0.6}W_{0.4}O_3$ composition heated to: (a) 800 °C – 1. TiO_2, 2. $Cs_{0.30}Ti_{0.004}W_{0.94}O_3$, 3. $Cs_{0.30}Ti_{0.13}W_{0.87}O_3$ (scale bar = 50 μm) and (b) 1200 °C – 1. $Cs_{0.29}Ti_{0.12}W_{0.87}O_3$ 2. fibrous $Cs_{0.25}Ti_{0.16}W_{0.85}O_3$, 3. $Cs_{0.24}Ti_{0.15}W_{0.86}O_3$ (scale bar = 500 μm). The numbers represent points at which EDS analyses were performed.

the region around 14.6°2θ. Numerous low angle harmonic reflections were also identified in this pattern (see expanded region top left). Attempts to model these patterns with multiple HTB components in a combination of space groups *P6/mmm*, *P63/mcm*, or $P6_322$ did not yield satisfactory refinements. While it was not possible to categorically rule out the existence of such phases as judged from the XRD patterns, it is worth remarking that an extensive search of the PDF database revealed a striking similarity between the experimental pattern of the $x = 0$ sample with that of $Cs_4W_{11}O_{35}$ (PDF 51-1851) for which no structure was available. On the other hand, the low angle harmonic reflections are also characteristic of intergrowth tungsten bronze structures which have been shown to have *a*-dimensions of about 34 Å [25].

As the TiO_2 precursor concentration in the initial compositions was increased the patterns became 'cleaner', and by about $x = 0.2$–0.3, phase pure bronze phases were obtained in addition to unreacted precursor. From these results it can therefore be concluded that temperatures equal to and above 1000 °C and initial compositions with $x \geqslant 0.2$ are required to afford single tungsten bronze phases. Phase assemblages of these compositions were all refined satisfactorily in space group *P63/mcm*. A general feature of all $Cs_yM_xW_{1-x}O_3$ compositions examined was that at low temperatures, where multiple phases were observed in the XRD patterns, Cs was exclusively partitioned into two main Ti-containing phases. One of these possessed a fibrous morphology, a low value of x (M concentration) and high value of y (Cs concentration). The other possessed an irregular morphology, lower y value and a higher x value. It must be noted though, that at higher temperatures a phase pure XRD pattern was observed and this was in turn supported by cross-sectional SEM analysis.

4.2. Cesium leaching

Initial studies of cesium leachability were conducted at 90 °C for 7 days with a series of Ti-substituted HTB phase assemblages prepared at temperatures between 600 and 1300 °C. The results from these investigations showed that the fraction of Cs leached from the solids was extremely low for each calcination temperature and that there was a general decrease in leachability as heating temperature was increased (Fig. 6 – ◆). The corresponding BET surface area measured for the 10–35 μm fractions revealed considerable porosity for calcination temperatures below about 800 °C. Furthermore, a clear trend was observed between the surface area and the fraction of Cs leached as might be expected (Fig. 6 – ●). That the fraction of Cs leached trends with surface area was not unexpected but it is surprising that the correlation is so good. This correlation indicates that variations within the phase assemblages produced at different temperatures have a minor impact on leaching. That is, it makes little difference whether anatase and/or rutile are present or if the sample is phase pure HTB or PYR. It can also be concluded that the leachability of the Cs-containing HTB and PYR phases present must be comparable.

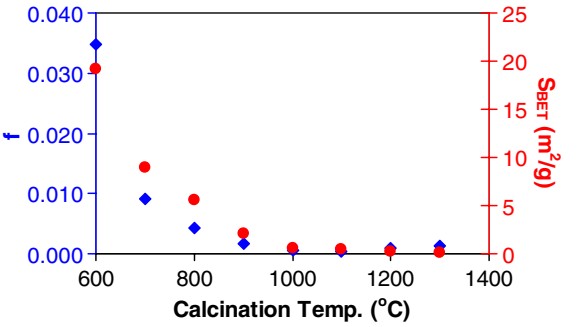

Fig. 6. Fractional Cs loss (◆) and BET surface area (●) from $Cs_{0.3}Ti_{0.6}W_{0.4}O_3$ compositions heated to increasing temperatures.

The leached fraction of Cs ranged from about 4×10^{-2} to 4×10^{-4}, a variation of about two orders of magnitude. Since the lowest fractional Cs loss was observed at temperatures at or above 1000 °C, we opted to explore a range of HTB compositions (M = Nb, Zr, Ti; $x = 0.05$–1) heated to this temperature. Recall that in the case of Ti substitution where $x = 0.6$, almost phase pure compounds were produced at this temperature (Fig. 5(g)).

The leachability of these compositions was again conducted on 10–35 μm samples at 90 °C for 7 days with the results presented in Fig. 7. It is clear that for this series of materials the best performance was obtained when Ti and Nb were the co-framework elements. The poorest performance for the bronze-based waste form powders was obtained for M = Zr. However, even $x < 0.4$ compositions of this substituent displayed superior performance to that of the reference hollandite materials prepared by either hot uniaxial pressing (HUPing) or sintering (SIN) under the given conditions. The impressive performance of the bronzoid materials is highlighted even further if one compares the

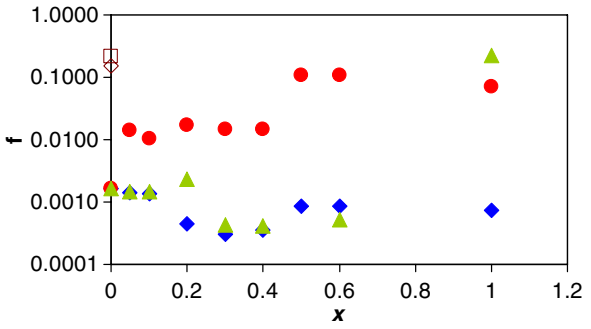

Fig. 7. Fraction of Cs leached from waste form powders with composition $Cs_{0.3}M_xW_{1-x}O_3$ heated to 1000 °C in air for 2 h where x varies from 0 to 1. M = Nb (◆), Zr (●), Ti (▲). Data for reference Cs-hollandite samples prepared by sintering in air (□) and hot uniaxial pressing (◇) respectively, are included for comparison.

surface area of the 10–35 μm fractions of the individual compositions. The hot uniaxially pressed (HUPed) Cs-hollandite had a BET surface area of only 0.009 m^2/g and $f = 0.22$ while the sintered Cs-hollandite had a BET surface area of 0.96 m^2/g and $f = 0.15$. In comparison all of the bronzoid waste form materials had BET surface areas that were comparable with the sintered Cs-hollandite while f was up to two orders of magnitude lower under the given conditions. Moreover, there was no particular correlation with BET surface area and f which suggests that any variation in fractional loss observed was entirely due to crystallochemical and compositional variations.

With regard to the Zr-containing compositions, there was an increase in the fractional Cs loss of about one order of magnitude as x was increased above 0.4. We have found that the phase assemblage of the Zr-containing compositions basically mimics that of the Ti-containing compositions and was comprised of Zr-substituted HTB, PYR and ZrO_2. For the Ti-containing compositions there was a dramatic increase in the fractional Cs loss from 5×10^{-4} to 0.2 as x was increased from 0.4 to 1. The value of 0.2 matches that of the titanate hollandites. The end member for the Ti-compositions was matched to orthorhombic $Cs_2Ti_6O_{13}$ (PDF 38-0170). Noteworthy is the fact that the Nb-containing compositions did not suffer such a dramatic increase in fractional loss for $x = 1$. Even after extensive SEM analysis, no HTB or PYR phases were observed in the $Cs_{0.3}NbO_3$ phase assemblage and we have been unable to match the XRD pattern of this composition to any in the PDF database. These results underscore the remarkably low inherent leachability of the Nb-, Zr-, and Ti-containing bronzoid compounds.

To facilitate comparison with other waste form materials it is necessary to carry out leaching experiments using the MCC-1 protocol since this is the most ubiquitous. To achieve this with the present compositions it was necessary to form consolidated masses. Melting the dried precursor powder was possible at temperatures above about 1100 °C, depending on the exact composition. The mass of highly crystalline material produced by melting was sufficiently robust to allow the production of polished disks for the MCC-1 test. MCC-1 leach data for the various tungstate compositions together with that for the reference Cs-hollandite samples is reported in Fig. 8. The normalized Cs losses at 90 °C in de-mineralized water were worst for the Mo-containing phases and are due to the formation of soluble Cs-rich molybdates. It should be noted that the Cs leached fraction and the normalized losses for the melted compounds are much higher than observed for the Cs-saturated HTB adsorbent phase (see Part 1). We propose that this is due to the much higher level of Mo in these melted compositions. The normalized losses for the other melted composition were generally excellent in comparison to the reference titanate phases. Performance was exceeded only by the sintered hollandite phase at leaching times greater than about 20 days.

Plots of the cumulative fraction of Cs lost as a function of time for selected substitutional elements allowed fitting of the leach data to a particular rate law (Fig. 9). For the unsubstituted and Ti-substituted compositions good fits were obtained using a

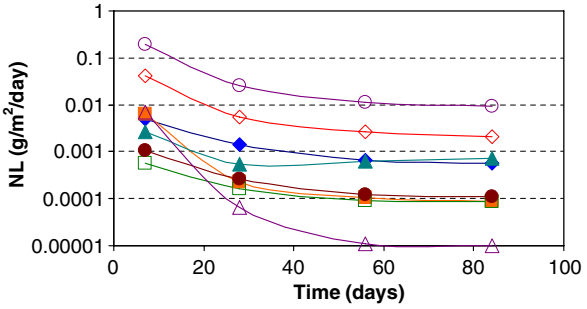

Fig. 8. Normalized Cs losses (NL) from a variety of compositions melted at 1300 °C determined using the MCC-1 protocol. $Cs_{0.3}WO_3$ (◆), $Cs_{0.3}Mo_{0.2}W_{0.8}O_3$ (○), $Cs_{0.3}Zr_{0.2}W_{0.8}O_3$ (◇), $Cs_{0.3}Ti_{0.2}W_{0.8}O_3$ (■), $Cs_{0.3}Ta_{0.2}W_{0.8}O_3$ (●), $Cs_{0.3}Nb_{0.2}W_{0.8}O_3$ (□), $Ba_{0.9}Cs_{0.3}Al_{2.1}Ti_{5.9}O_{16}$ (HUP) (▲), $Ba_{0.9}Cs_{0.3}Al_{2.1}Ti_{5.9}O_{16}$ (SIN) (△).

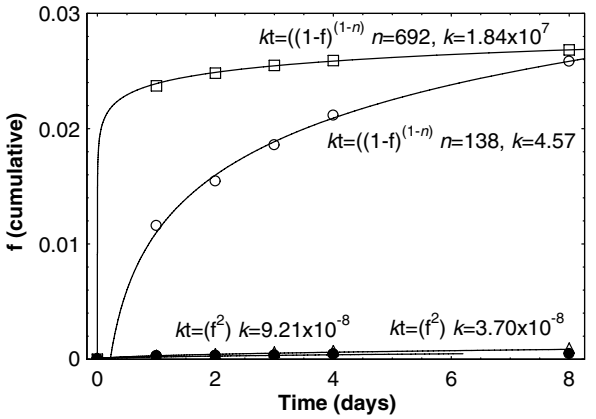

Fig. 9. Cumulative fractional Cs loss as a function of time for selected $Cs_{0.3}M_{0.2}W_{0.8}O_3$ compositions melted at 1300 °C fitted to deceleratory rate laws. $Ba_{0.9}Cs_{0.3}Al_{2.1}Ti_{5.9}O_{16}$ (HUP) (●), $Cs_{0.3}Nb_{0.2}W_{0.8}O_3$ (△), $Cs_{0.3}Ti_{0.2}W_{0.8}O_3$ (□), $Cs_{0.3}WO_3$ (○). Fitted parameters are shown in graph.

deceleratory dissolution rate law $kt = (1 - f)^{(1-n)}$ as given by Blesa et al. [26] A similar expression could not be fitted to the data for the Nb-substituted tungstate or the sintered hollandite data, which required fitting to a $kt = f^2$ law. Clearly, solution saturation effects are not relevant in regard to highly soluble Cs^+ in explaining this apparent difference.

The decay of ^{137}Cs involves the emission of β-particles ($0.51 \leqslant$ energy $E \leqslant 1.17$ MeV), γ rays ($E \approx 0.6$ MeV) and the transmutation of Cs to stable Ba. Therefore, Cs host waste forms must be stable under (β, γ)-irradiation, chemically durable and must tolerate the changes in chemistry resulting from the conversion of radiogenic Cs to stable Ba. To test the effects that partial conversion of Cs to Ba might have on the $Cs_yM_xW_{1-x}O_3$ system, a series of $Ba_{0.1}WO_3$ compositions were prepared and heated in air to temperatures in the range 600–1300 °C. The fractional Ba loss and normalized 7-day leach rates are reported in Table 2. The results demonstrated that Ba-containing tungstates were highly leach resistant in comparison to Ba-containing Cs-hollandite but the leachability increased with increasing calcination temperature.

Table 2
Fraction of Ba leached (f) and normalized release rates (NL) for $Ba_{0.2}WO_3$ compositions heated in air at increasing temperatures compared to Cs-hollandite

Sample	f	NL(Ba) (g/m^2/day)
$Cs_{0.10}Ba_{1.0}Al_{2.1}Ti_{5.9}O_{16}$	1.60×10^{-2}	6.60×10^{-3}
$Ba_{0.20}WO_3$ 600 °C	1.70×10^{-6}	2.38×10^{-9}
$Ba_{0.20}WO_3$ 800 °C	1.80×10^{-6}	1.64×10^{-8}
$Ba_{0.20}WO_3$ 1000 °C	5.50×10^{-6}	1.33×10^{-4}
$Ba_{0.20}WO_3$ 1300 °C	4.80×10^{-6}	1.34×10^{-4}

5. Discussion

We have previously reported the basic ion exchange properties of microporous hydrous tungsten bronze materials of general formula $Na_yMo_xW_{1-x}O_3 \cdot ZH_2O$ [1]. The selectivity of such materials for large cations such as Cs^+ and Sr^{2+} is a feature which may make them useful in a radioactive waste pretreatment context for the adsorption of radiogenic cesium and strontium. That such materials can be converted directly to leach resistant ceramics by calcination in air or by melting at relatively low temperatures with little volatilization of Cs adds to the attractiveness of such materials for nuclear applications as does the tolerance of the system to the presence of Mo (refer to Part 1). Since compositional flexibility is important in designing nuclear waste form ceramic systems we have addressed this issue in greater detail here. Particularly important is the influence that cation substitution into the basic host framework has in modifying the solubility. We have ignored, for the time being, the influence that thermal processing can have on crystallization sequences and crystallite sizes and focused on the inherent leachability of the various compositions. Our data on the hexagonal tungsten bronze supports earlier studies of cubic tungsten bronze systems [27] which suggested that the tungsten oxide system contained significant scope for including a wide array of substitutional elements, and which placed the solid solution limit at about $0.2(x)$. Our results show that inclusion of other substitutional elements does result in modification of the chemical durability. In some instances significant improvement was observed, while in others, deleterious effects were observed. In comparison with other substitutional elements, the leachability of Mo-containing compositions was relatively poor; however, in no case was catastrophic leachability observed.

A search for Cs-containing tungsten bronze phases in the ICSD database revealed a paucity of such phases and these are summarized in Table 3. $Cs_{0.23}Nb_{0.09}W_{0.91}O_3$ and $Cs_{0.29}Nb_{0.1}W_{0.9}O_3$ were reported recently by Dey et al. [28] and Zr, Nb and Ti containing pyrochlores with general formula $A(B_{0.5}B'_{1.5})O_6$ (A = K, Rb, Cs, Tl; B = Ti, Zr; B′ = Te, W) have been known for some time [24]. In this later study, a trend was observed between

Table 3
Summary of Cs-containing tungstates

Composition	ICSD	System	Space group	a (Å)	b (Å)	c (Å)	References
Bronze phases							
$Cs_{0.07}WO_3$	28261	Ortho	$P22_12$	34.85	7.33	7.758	Hussain [29]
$Cs(Mo_{0.95}W_{0.05})_7O_{21}$	69806	Ortho	*Pnma*	17.638	5.448	17.945	Zocchi et al. [30]
$Cs_{0.29}WO_3$	56223	Hex	$P6_322$	7.412	7.412	7.60	Prinz et al. [31]
$Cs_{0.3}WO_3$ (red)	72618	Hex	*P63/mcm*	7.4049	7.4049	7.6098	Oi et al. [32]
$Cs_{0.287}W_{0.95}O_3$ (oxid)	72619	Hex	*P63/mcm*	7.4012	7.4012	7.6728	Oi et al. [32]
$Cs_{0.20}WO_3$	100192	Hex	*P63/mcm*	7.4203	7.4203	7.5674	Kihlborg and Hussain [33]
$Cs_{0.32}WO_3$	100193	Hex	*P63/mcm*	7.4116	7.4116	7.5981	Kihlborg and Hussain [33]
$Cs_{0.23}Nb_{0.09}W_{0.91}O_3$	409638	Hex	*P63/mcm*	7.3998	7.3998	7.5732	Dey [28]
$Cs_{0.29}Nb_{0.1}W_{0.9}O_3$	409639	Hex	*P63/mcm*	7.3992	7.3992	7.5867	Dey [28]
Pyrochlore phases							
$CsTaWO_6$	18092	Cubic	*Fd-3m*	10.36	10.36	10.36	Babel et al. [34]
$CsVWO_6$	18091	Cubic	*Fd-3m*	10.18	10.18	10.18	Babel et al. [34]
$CsNbWO_6$	18093	Cubic	*Fd-3m*	10.38	10.38	10.38	Babel et al. [34]
$CsSbWO_6$	9527	Cubic	*Fd-3m*	10.279	10.279	10.279	Michel et al. [35]
$CsTi_{0.5}W_{1.5}O_6$	202945	Cubic	*Fd-3m*	10.271	10.271	10.271	Castro et al. [24]
$CsZr_{0.5}W_{1.5}O_6$	202947	Cubic	*Fd-3m*	10.4109	10.4109	10.4109	Castro et al. [24]
$CsHf_{0.5}W_{1.5}O_6$	202948	Cubic	*Fd-3m*	10.3906	10.3906	10.3906	Castro et al. [24]
$CsCr_{0.333}W_{1.667}O_6$	23428	Cubic	*Fd-3m*	10.264	10.264	10.264	le Flem [36]

the a-dimension and the ionic radius of the A cation and the B–B′ distance. On the contrary, no hexagonal tungsten bronze oxide compounds containing Zr, Ti or Ta have been described in the literature and nor do they appear in the ICSD. Here we have refined the structures of such materials where single-phase patterns were obtained. This was achieved for Zr^{4+}, Nb^{5+}, Ta^{5+} and Ti^{4+}-substituted materials with $x = 0.2$ and $y = 0.3$. Our observations suggest that the value of $x = 0.2$ is close to the solid solution limit for the M element in the HTB system. Further examination of the refinement results for these phases demonstrates a trend between the ionic radius of the substituting element and the a-dimension but the correlation is not linear (Fig. 10). This could possibly be due to the fact that the value of the a-dimension also depends on the Cs content of the tunnels, which varies slightly in the samples produced. When these unit cell a-dimensions are compared in the light of the leaching data shown in Fig. 7, there appears to be no trend between the leachability of the $Cs_{0.3}M_{0.2}W_{0.8}O_3$ compositions and their a-dimension, which in turn suggests that extraction of Cs is not due to any ion-exchange process but is more likely to be determined by the thermodynamic stability of the framework.

In their study of the Cs_2O–WO_2–WO_3 system Cava and Roth [23] identified a number of cesium

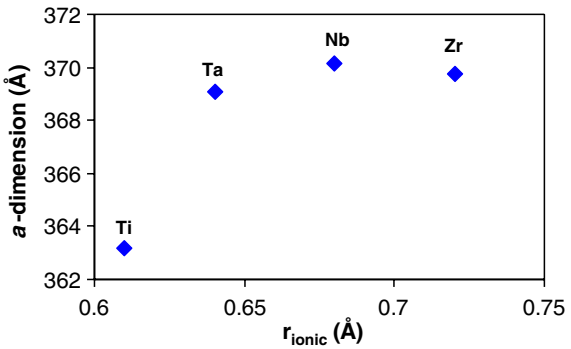

Fig. 10. Trend between ionic radius of M element in composition $Cs_{0.3}M_xW_{1-x}O_3$ and the unit cell a-dimension. $x = 0.2$; M = Ti ($r = 0.61$ Å), Ta ($r = 0.64$ Å), Nb ($r = 0.68$ Å), Zr ($r = 0.71$ Å).

tungstate phases including new HTB- ($Cs_{8.5}W_{15}O_{46}$) and PYR-type oxides ($Cs_2W_2O_6$) as well as a homologous series of compounds intermediary between HTB and PYR when heating was carried out in vacuum. While the present study has exclusively examined heating in air due to its simplicity, it is clear that the marginal increase in complexity deriving from heating under reducing conditions can potentially result in a rich phase chemistry in the Cs–M–W system. This study suggests that all such compounds should display excellent resistance to chemical dissolution.

6. Conclusion

The process used in this work to make Cs–M–W compositions in which Cs is exclusively retained by HTB phases is exceedingly simple and forgiving. Furthermore, a high tolerance to the inclusion of other oxides has been demonstrated. It has been possible to prepare high quality materials where complete partitioning of Cs into the durable phases has been achieved by doing little more than combining tungstic acid, Cs nitrate and other oxides in an open crucible with little or no mixing followed by relatively mild heating in air. Very little Cs can be leached from sintered or melted HTB-based waste form materials under the testing conditions employed and the performances achieved are on par with titanate-based waste form materials. To our knowledge this is the first demonstration of the preparation of bronze materials by this simple strategy.

References

[1] C.S. Griffith, V. Luca, Chem. Mater. 16 (2004) 4992.
[2] C.S. Griffith, V. Luca, P. Yee, F. Sebesta, Sep. Sci. Technol. 40 (2005) 1781.
[3] V. Luca, E. Drabarek, C.S. Griffith, H. Chronis, J. Foy, Mater. Res. Symp. Proc. 807 (2004) 303.
[4] W. Lutze, R.C. Ewing, Radioactive Waste Forms for the Future, North-Holland, Elsevier, Amsterdam, 1988 (Chapter 4).
[5] K.D. Reeve, A.E. Ringwood, Radioactive waste management, in: Proceedings of the International Conference, 1984, p. 307.
[6] V.M. Oversby, A.E. Ringwood, Nucl. Chem. Waste Manage. 2 (1981) 201.
[7] L.P. Hatch, Am. Scientist 41 (1953) 410.
[8] G.J. McCarthy, M.T. Davidson, Am. Ceram. Soc. Bull. 54 (1975) 782.
[9] G.J. McCarthy, Proceedings of the Rare Earth Research Conference, 12th, 1976, p. 665.
[10] G.J. McCarthy, M.T. Davidson, Am. Ceram. Soc. Bull. 55 (1976) 190.
[11] R.G. Dosch, Sandia National Laboratory, SAND-75-5601, 1975.
[12] J. Davidovitz, United States Patent 5 349 118.
[13] M.Y. Khalil, E. Merz, J. Nucl. Mater. 211 (1994) 141.
[14] A. Mathur, United States Patent 5 494 863.
[15] D.J. Wronkiewicz, S.F. Wolf, T.S. DiSanto, Mater. Res. Soc. Symp. Proc. 412 (1996) 345.
[16] D.J. Wronkiewicz, X. Feng, N.R. Brown, T.S. DiSanto, Emerging Technologies in Hazardous Waste Management IV, The American Chemical Society, Atlanta, GA, 1984.
[17] G.H. Beall, H.L. Rittler, Adv. Ceram. 4 (1982) 301.
[18] D.M. Strachan, W.W. Schulz, ARH-SA-246, 1976.
[19] W. Lutze, J. Borchardt, A.K. De, Sci. Basis Nucl. Waste Manage. (1979) 69.
[20] B. Gerand, G. Nowogrocki, J. Guenot, M. Figlarz, J. Solid State Chem. 29 (1979) 429.
[21] M. Figlarz, Prog. Solid State Chem. 19 (1989) 1.
[22] L. Seguin, M. Figlarz, R. Cavagnat, J.-C. Lassegues, Spectrochim. Acta A 51 (1995) 1323.
[23] R.J. Cava, R.S. Roth, T. Siegrist, B. Hessen, J.J. Krajewski, W.F.J. Peck, J. Solid State Chem. 103 (1993) 359.
[24] A. Castro, I. Rasines, X.M. Turrillas, J. Solid State Chem. 80 (1989) 227.
[25] C. Grenthe, M. Sundberg, V.P. Filonenko, I.P. Zibrov, J. Solid State Chem. 154 (2000) 466.
[26] M.A. Blesa, P.J. Morando, A.E. Regazzoni, Chemical Dissolution of Metal Oxides, CRC Press, Boca Raton, 1993.
[27] P. Labbe, Key Eng. Mater. 68 (1992) 293.
[28] K.R. Dey, Th.R. Gesing, C.H. Ruscher, A. Hussain, Z. Kristallogr. 217 (2002) 416.
[29] A. Hussain, Chem. Scr. 11 (1977) 224.
[30] M. Zocchi, L.E. Depero, F. Zocchi, J. Solid State Chem. 92 (1991) 18.
[31] H. Prinz, U. Mueller, M.L. Ha-Eierdanz, Z. Anorg. Allg. Chem. 609 (1992) 95.
[32] J. Oi, A. Kishimoto, T. Kudo, J. Solid State Chem. 103 (1993) 176.
[33] L. Kihlborg, A. Hussain, Mater. Res. Bull. 14 (1979) 667.
[34] D. Babel, G. Pausewang, W. Viebahn, Z. Naturforsch. B 22 (1967) 1219.
[35] C. Michel, D. Groult, B. Raveau, Mater. Res. Bull. 8 (1973) 201.
[36] G. le Flem, R. Salmon, C.R. Hebd. Seances Acad. Sci. C: Sci. Chim. 271 (1970) 1182.